IMMUNOLOGY

Efficient aortic lymphatic drainage is necessary for atherosclerosis regression induced by ezetimibe

Kim Pin Yeo[1,2], Hwee Ying Lim[1,2], Chung Hwee Thiam[1,2], Syaza Hazwany Azhar[1,2], Caris Tan[3], Ya Tang[1,2], Wei Qiang See[1,2], Xuan Han Koh[1,2], Ming Hao Zhao[1,2], Meow Ling Phua[4], Akhila Balachander[4], Yingrou Tan[4]*, Sheau Yng Lim[1,2], Hui Shang Chew[1,2], Lai Guan Ng[1,2], Veronique Angeli[1,2†]

A functional lymphatic vasculature is essential for tissue fluid homeostasis, immunity, and lipid clearance. Although atherosclerosis has been linked to adventitial lymphangiogenesis, the functionality of aortic lymphatic vessels draining the diseased aorta has never been assessed and the role of lymphatic drainage in atherogenesis is not well understood. We develop a method to measure aortic lymphatic transport of macromolecules and show that it is impaired during atherosclerosis progression, whereas it is ameliorated during lesion regression induced by ezetimibe. Disruption of aortic lymph flow by lymphatic ligation promotes adventitial inflammation and development of atherosclerotic plaque in hypercholesterolemic mice and inhibits ezetimibe-induced atherosclerosis regression. Thus, progression of atherosclerotic plaques may result not only from increased entry of atherogenic factors into the arterial wall but also from reduced lymphatic clearance of these factors as a result of aortic lymph stasis. Our findings suggest that promoting lymphatic drainage might be effective for treating atherosclerosis.

INTRODUCTION

Atherosclerosis is a chronic inflammatory disease of the arterial wall, and the associated cardiovascular complications represent the most common cases of death in developed countries. The disease develops gradually and silently over decades, progressively evolving from fatty streaks characterized by macrophages loaded with cholesterol ester to advanced plaques with more complex cellular composition, lipid pools, and necrotic debris (*1*). During disease progression, continuous recruitment of monocytes, deposition of cholesterol crystals, and undesirable immunity against cholesterol-associated apolipoprotein trigger and sustain chronic inflammation in the arterial wall. Although much emphasis has been placed on intima where atherosclerosis develops, it is of great importance to consider the effect of adventitial remodeling including increased immune cell accumulation, lymphangiogenesis, and neovascularization during intimal lesion formation and progression because intima and adventitia are in close proximity and cross-talk (*2*).

The lymphatic circulation that runs in conjunction with the blood circulation plays an essential role in maintaining body fluid homeostasis, immunity, and lipid transport (*3*). The lymphatic system is composed of an extensive network of lymphatic vessels and interconnected lymph nodes (LNs). To accomplish its functions, it must transport lymph from the interstitial spaces into and through the lymphatic vessels, the thoracic duct, and back to the blood circulation. This movement of lymph containing lipids, cells, macromolecules, and fluid is first collected by initial or capillary lymphatic vessels. Lymph is then transported to larger lymphatic vessels, collecting or collector vessels, in which initial lymphatic vessels converge. Unlike initial lymphatic vessels, collecting vessels exhibit circumferential smooth muscle cell coverage and luminal valves that propel and maintain unidirectional flow. Lymphangiogenesis, the formation of lymphatic vessels from preexisting ones, has been associated with experimental and clinical inflammatory diseases including atherosclerosis (*4*–*8*). Increased adventitial lymphatic density correlates with intimal thickness, notably in advanced or ruptured atherosclerotic lesions (*5*, *6*, *9*). In contrast, intimal lymphangiogenesis is very rare in atherosclerotic human coronary arteries (*10*, *11*) despite high expression of the lymphangiogenic factor vascular endothelial growth factor–C (VEGF-C) (*12*). Most of these reports revealing an association between lymphangiogenesis and atherosclerosis evaluate lymphatic vessel number, size, or density on tissue sections but fail to provide data on the functionality of the lymphatic vessels draining the aorta. However, such functional studies are fundamental to determine whether arterial lymphangiogenesis is a component of the pathology or a productive attempt to limit atherosclerosis progression by increasing lymph efflux and hence drainage of lipids and immune cells, and represents a therapeutic target for this cardiovascular disease. Therefore, we developed new tools to assess the functionality of aortic lymphatic vessels in experimental atherosclerosis and further defined the contribution of lymphatic drainage in atherogenesis.

RESULTS

Expansion of adventitial lymphatic vessels is associated with atherosclerotic plaque progression

The existence of aortic lymphatic vessels in mice has been described, but their exact topography on the entire aorta has not been illustrated (*13*, *14*). Thus, we characterized the lymphatic vessel network in the normal mouse aorta using whole-mount staining. The presence of LYVE-1$^+$ blind-ended initial lymphatics was consistently observed in the adventitia of the aortic sinus, thoracic aorta, and abdominal

[1]Immunology Translational Research Programme, Department of Microbiology and Immunology, Yong Loo Lin School of Medicine, National University of Singapore, Singapore, Singapore. [2]Immunology Programme, Life Sciences Institute, National University of Singapore, Singapore, Singapore. [3]Histology Core Facility, Life Sciences Institute, National University of Singapore, Singapore, Singapore. [4]Singapore Immunology Network (SIgN), Agency for Science, Technology and Research (A*STAR), Biopolis, Singapore, Singapore.
*Present address: Department of Research, National Skin Centre, 1 Mandalay Rd, Singapore 308205, Singapore.
†Corresponding author. Email: micva@nus.edu.sg

aorta, whereas they were rarely detected in the aortic arch (fig. S1, A to D). In the thoracic aorta, lymphatic vessels ran alongside the aorta, with some being closer to the azygous vein, while others ran in parallel to the adjacent periadventitial adipose tissue (fig. S1C). Lymphatic vessels also appeared to encircle the intercostal arteries. Lymphatic vessels in the abdominal aorta were in close proximity to the inferior vena cava (IVC) (fig. S1D). Immunofluorescent staining of aortic sinus and abdominal aorta cross sections for additional markers including collagen I, VEGF receptor–3 (VEGFR-3), podoplanin, prox-1, and macrophage CD68 further confirmed that LYVE-1$^+$ structures were initial lymphatic vessels residing in type I collagen–rich adventitial and periadventitial tissues and were not LYVE-1$^+$ macrophages (fig. S1, E to G) (*15*).

An association between lymphangiogenesis and atherosclerosis has been reported in mice and humans (*4*, *9*, *11*). However, these studies did not assess the temporal remodeling of lymphatic vessels during the progression of atherosclerosis. Thus, we analyzed qualitative and quantitative changes of lymphatic vessels in the aortic sinus and abdominal aorta of apolipoprotein-E–deficient (*Apoe*$^{-/-}$) mice fed a high-fat diet (HFD) from 8 to 32 weeks of age. Microscopic analysis of aortic sinus whole mounts revealed the expansion of the lymphatic vessel network and lymphatic sprouting in *Apoe*$^{-/-}$ mice at 24 weeks of age (Fig. 1, A and B), suggesting the presence of lymphangiogenesis. The increase in adventitial lymphatic vessel number was evident in aortic sinus sections from *Apoe*$^{-/-}$ mice by 20 to 22 weeks and remained high at 32 weeks of age (Fig. 1, C and D). Lymphangiogenesis was further demonstrated by a fourfold increase in *Prox-1* gene expression in the adventitia of *Apoe*$^{-/-}$ aortic sinus (Fig. 1E). The expression of the proliferative marker Ki67 was mainly observed in the dilated lymphatic vessels (Fig. 1F). The lymphangiogenic response positively correlated with atherosclerotic plaque progression expressed as percentage of plaque ($r = 0.8314$, $P < 0.0001$) (Fig. 1G). Notably, the increase in lymphatic vessel number became statistically significant when plaque area occupied more than 30% of the aortic lumen (Fig. 1H), and lymphatic lumen area was quantitatively and significantly larger in the atherosclerotic aortic sinus (Fig. 1, I and J). Similar to the observations in the aortic sinus, the lymphatic vessel network also expanded in the abdominal aorta of *Apoe*$^{-/-}$ mice as evident from whole-mount staining and the significant increase in lymphatic vessel number when plaque area occupied more than 30% of the aortic lumen (Fig. 1, K to N). As expected, atherosclerosis progression was also accompanied by the expansion of vasa vasorum in the adventitia of aortic sinus and abdominal aorta (Fig. 1, A and L, and fig. S2, A to F). However, we noted that angiogenesis occurred earlier than lymphangiogenesis and surpassed it during disease progression, resulting in the imbalance of the ratio of blood vessel to lymphatic vessel numbers (fig. S2, C and F). Similar results for lymphangiogenesis and angiogenesis were obtained in mouse deficient in low-density lipoprotein receptor (*Ldlr*$^{-/-}$), another mouse model of atherosclerosis, further supporting the physiological relevance of our observations (fig. S3). Together, we provide evidence using two atherosclerotic animal models that advanced, but not early, atherosclerotic lesions are accompanied by the growth of lymphatic vessels.

Reduced lymphangiogenesis is associated with regression of atherosclerotic plaque

We next studied lymphangiogenesis during the regression of atherosclerosis in *Apoe*$^{-/-}$ mice induced by treatment with ezetimibe, which has been reported to reduce plasma cholesterol by targeting the cholesterol transport protein Niemann-Pick C1-like protein (NPC1L1) expressed by enterocytes and hepatocytes and to decrease atherosclerotic plaque size and inflammation (*16*–*18*). We analyzed aortic initial lymphatic changes following ezetimibe treatment, which was initiated either before or after the onset of lymphangiogenesis and continued for 12 or 16 weeks, respectively (Fig. 2A). Consistent with other (*16*) and our previous reports (*19*, *20*), total cholesterol levels and atherosclerotic plaque areas were markedly reduced in ezetimibe-treated *Apoe*$^{-/-}$ mice as compared to the vehicle-treated *Apoe*$^{-/-}$ mice (fig. S4, A to E). Evaluation of lymphatic vessels in aortic sinus whole mounts of *Apoe*$^{-/-}$ mice revealed a reduction in the lymphatic vessel network and lymphatic sprouts 12 weeks after ezetimibe treatment (Fig. 2B). Quantification of CD31$^+$LYVE-1$^+$ vessel in aortic sinus cross sections showed that ezetimibe treatment reduced the number of lymphatic vessels in *Apoe*$^{-/-}$ mice, which was comparable to that in wild-type (WT) mice (Fig. 2, C and D). Initial lymphatic vessels were also less hyperplasic after ezetimibe treatment (Fig. 2B), as confirmed by the decrease in lymphatic lumen area (Fig. 2E). Treatment with ezetimibe after the onset of lymphangiogenesis also significantly reduced the number of lymphatic vessels in the aortic sinus in *Apoe*$^{-/-}$ mice (Fig. 2, F and G) but did not affect lymphatic lumen area (Fig. 2H). We also noted that the two different ezetimibe treatment regimes affected angiogenesis (fig. S4, F and G). These data demonstrate that lymphangiogenesis subsides during the regression of atherosclerotic plaques induced by lowering plasma cholesterol. We next investigated whether the lymphangiogenic factor VEGF-C accounts for lymphangiogenesis observed in *Apoe*$^{-/-}$ mice. Consistent with a previous report (*21*), we showed that plasma VEGF-C levels and aortic *Vegf-c* gene expression were significantly increased in *Apoe*$^{-/-}$ mice compared to WT mice and this was reversed upon treatment with ezetimibe (fig. S5, A and B). Furthermore, adventitial lymphatic vessel numbers were increased in *Apoe*$^{-/-}$ mice by the administration of a recombinant form of VEGF-C protein with a substitution of Cys^{156} by a serine residue (VEGFC-156S) but not VEGF-C when administrated before the onset of lymphangiogenesis (fig. S5C). The effect of VEGFC-156S was independent of plasma cholesterol levels (fig. S5D). Because VEGFC-156S is only active toward VEGFR-3 (*22*), we went on to block VEGFR-3 in *Apoe*$^{-/-}$ mice before the onset of lymphangiogenesis and we showed reduced adventitial lymphatic vessel numbers without affecting plasma cholesterol (fig. S5, E and F). These findings suggest that VEGF-C is a potential lymphangiogenic factor supporting adventitial lymphangiogenesis during atherosclerosis.

Aortic lymphatic drainage is impaired during atherosclerosis

To understand the functional significance of lymphangiogenesis in atherosclerosis, we investigated whether the observed lymphatic remodeling in the adventitia of the diseased aorta results in alteration of lymphatic drainage. One would expect that the expansion of the aortic lymphatic vessel network would enhance lymphatic transport and would be beneficial by clearing immune cells and inflammation. As a first approach, we determined whether the changes in lymphatic structure and number observed during atherosclerosis affect the accumulation of immune cells including dendritic cells (DCs) and T cells in the adventitia because they rely on functional lymphatics for their trafficking. A previous report in murine ear explants showed that DCs can sense CCL21 within a distance of 100 μm from a lymphatic vessel and increase their migratory velocity and

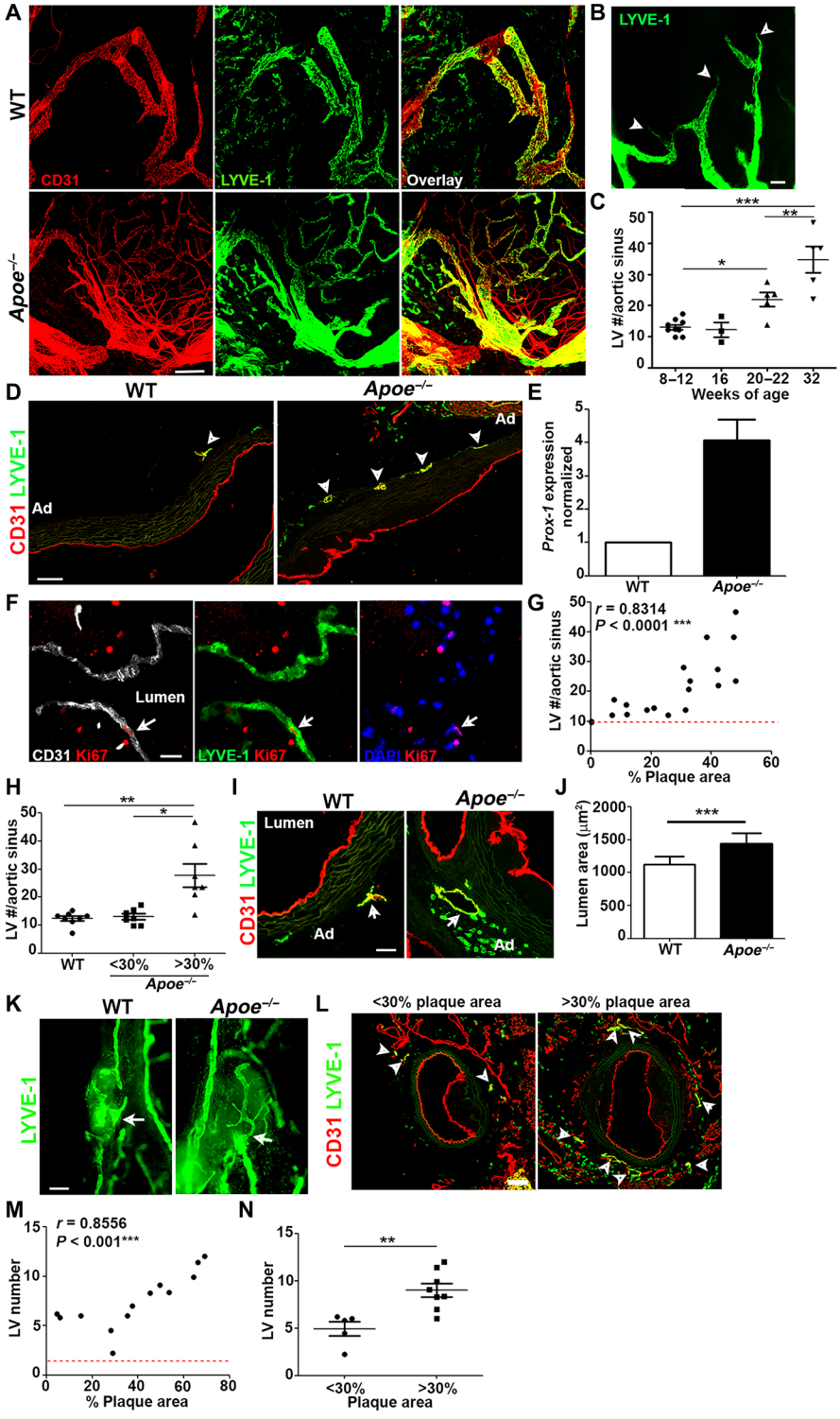

Fig. 1. Remodeling of lymphatic vessels on aortic wall during atherosclerosis. (**A**) Lymphatic vessels (LVs) were examined in whole-mount aortic sinuses from 24-week-old WT and *Apoe*$^{-/-}$ mice. Scale bar, 200 μm. (**B**) Lymphatic sprouts (arrowheads) were observed in *Apoe*$^{-/-}$ aortic sinus. Scale bar, 20 μm. (**C**) Adventitial LV number/aortic sinus was quantified across different ages. (**D**) More LVs (arrowheads) were observed in *Apoe*$^{-/-}$ mice. Ad, adventitia. (**E**) *Prox-1* mRNA expression was assessed in WT and *Apoe*$^{-/-}$ aortic sinuses. (**F**) LVs in *Apoe*$^{-/-}$ aortic sinus were costained with proliferative marker Ki67. Scale bar, 20 μm. (**G**) LV number was correlated with % plaque area. (**H**) LV number/aortic sinus was quantified in WT and *Apoe*$^{-/-}$ mice with less or >30% of plaque area. (**I**) LVs were more dilated in *Apoe*$^{-/-}$ than in WT mice. Scale bar, 20 μm. (**J**) Lymphatic lumen area was quantified in WT and *Apoe*$^{-/-}$ aortic sinuses. (**K**) Whole-mount and (**L**) cross-sectional abdominal aortic LVs from *Apoe*$^{-/-}$ mice were examined. Scale bar, 200 μm. (**M**) Correlation between LV number and % plaque area was analyzed. (**N**) LV number/abdominal aorta with less or >30% of plaque area was quantified in *Apoe*$^{-/-}$ mice. $n = 2$ to 8 mice. One-way ANOVA was used in (C) and (H), Mann-Whitney *U* test in (J), and Student's *t* test in (N).

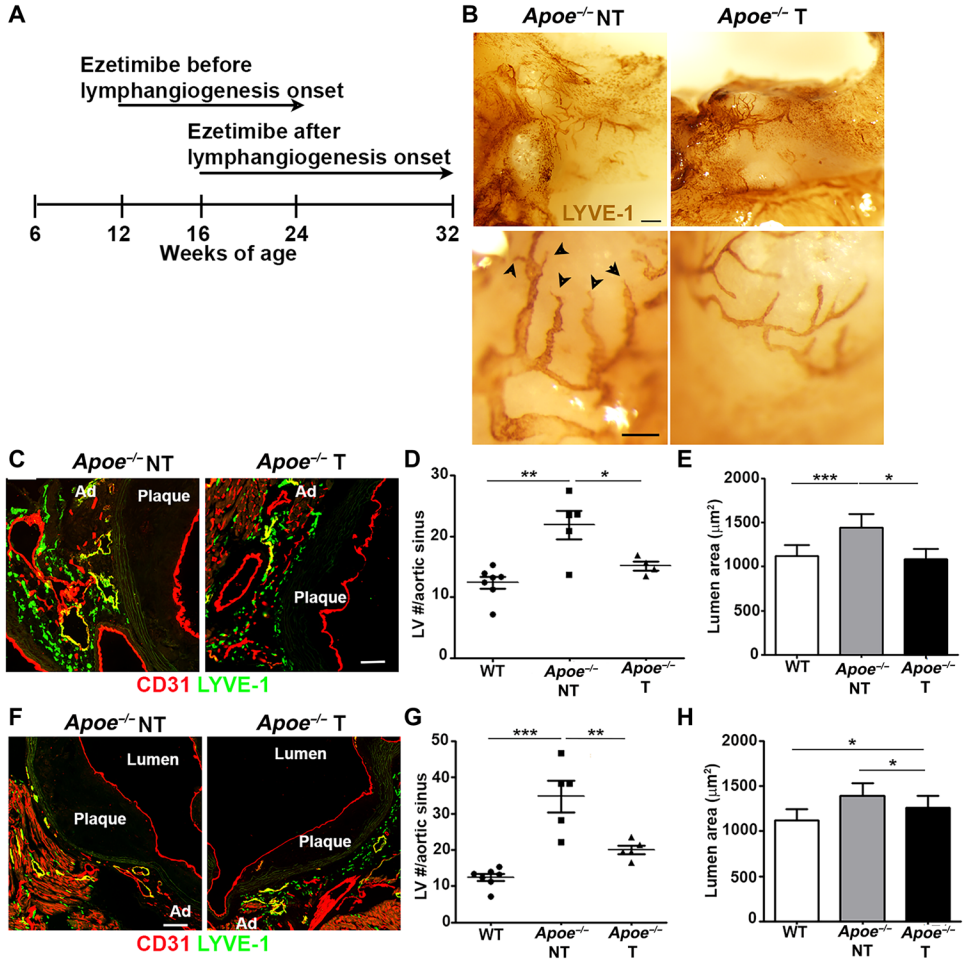

Fig. 2. Amelioration of atherosclerosis-associated lymphatic remodeling after ezetimibe treatment. (**A**) Schematic diagram of ezetimibe regime. WT and *Apoe*$^{-/-}$ mice were fed an HFD from 6 weeks of age. Ezetimibe was orally administered to 12- and 16-week-old *Apoe*$^{-/-}$ mice before and after lymphangiogenesis onset, respectively. Aortic sinuses were analyzed after (B to E) 12 and (F to H) 16 weeks of ezetimibe [treated (T)] or vehicle [nontreated (NT)] treatment. (**B**) LYVE-1 colorimetric whole-mount staining of aortic sinus was performed in NT and T *Apoe*$^{-/-}$ mice. Lymphatic sprouts (arrowheads). Scale bars, 1 mm (top) and 50 μm (bottom). (**C**) LV was examined in NT and T *Apoe*$^{-/-}$ aortic sinus after 12 weeks of treatment. Scale bar, 100 μm. (**D**) LV numbers and (**E**) LV lumen area/aortic sinus were quantified in NT WT, NT *Apoe*$^{-/-}$, and T *Apoe*$^{-/-}$ mice after 12 weeks of treatment. (**F**) LVs were examined in NT and T *Apoe*$^{-/-}$ aortic sinus after 16 weeks of treatment. Scale bar, 100 μm. (**G**) LV numbers and (**H**) LV lumen area/aortic sinus were quantified in NT WT, NT *Apoe*$^{-/-}$, and T *Apoe*$^{-/-}$ mice. $n = 4$ to 7 mice. One-way ANOVA was used for multiple group comparisons.

directedness toward the lymphatic vessel (*23*). Using this as guideline, we quantified the number of adventitial CD11c^{+} major histocompatibility complex class II–positive (MHCII^{+}) DCs and CD3^{+} T cells within 100 μm from initial CD31^{+}LYVE-1^{+} lymphatic vessels on aortic sinus cross sections. The analysis revealed a notable accumulation of both DCs and T cells in proximity of adventitial lymphatic vessels in *Apoe*$^{-/-}$ mice compared to WT mice, and this was reversed through treatment with ezetimibe (Fig. 3, A to H). In addition, we found that increased expression of inflammatory genes such as *interleukin-1*β (*IL-1*β), *tumor necrosis factor*–α (*TNF*-α), and *IL-6* in atherosclerotic aorta was reversed when atherosclerotic plaques and lymphangiogenesis regressed upon ezetimibe treatment (Fig. 3, I and J). These data led us to speculate that the lymphatic transport from the aorta may be compromised during atherosclerosis.

As a second and more direct approach to assess the functionality of adventitial lymphatic vessels in atherosclerotic aorta, we developed a quantitative method to measure specifically lymphatic transport of fluorescent tracer from the adventitia to the draining LNs. We targeted the abdominal aorta because the adventitia of abdominal aorta was more readily accessible for tracer injection as opposed to the aortic sinus. Optical tissue clearing of intact abdominal aorta together with IVC and iliac LNs facilitated the identification of the optimal site for tracer injection. IVC strongly stained for smooth muscle actin (SMA) as compared to the aorta (fig. S1D and Fig. 4A), and lymphatic vessels were again observed running alongside the aorta and between the aorta and IVC (fig. S1D; Fig. 4, A and B; and movie S1). On the basis of this observation, we decided to inject fluorescein isothiocyanate (FITC)–labeled dextran into the area between aorta and IVC located above the bifurcation of the iliac arteries (Fig. 4C). Fluorescence images and movie revealed that, upon injection, FITC-labeled dextran was taken up by adventitial lymphatic vessels and then drained either into the proximal iliac draining LNs or directly to renal LNs through efferent lymphatic vessel between aorta and IVC, the cisterna chyli, and eventually into the thoracic duct (Fig. 4C and movie S2). The lymph draining pathway is depicted in Fig. 4D. We next assessed the kinetic of FITC-labeled dextran

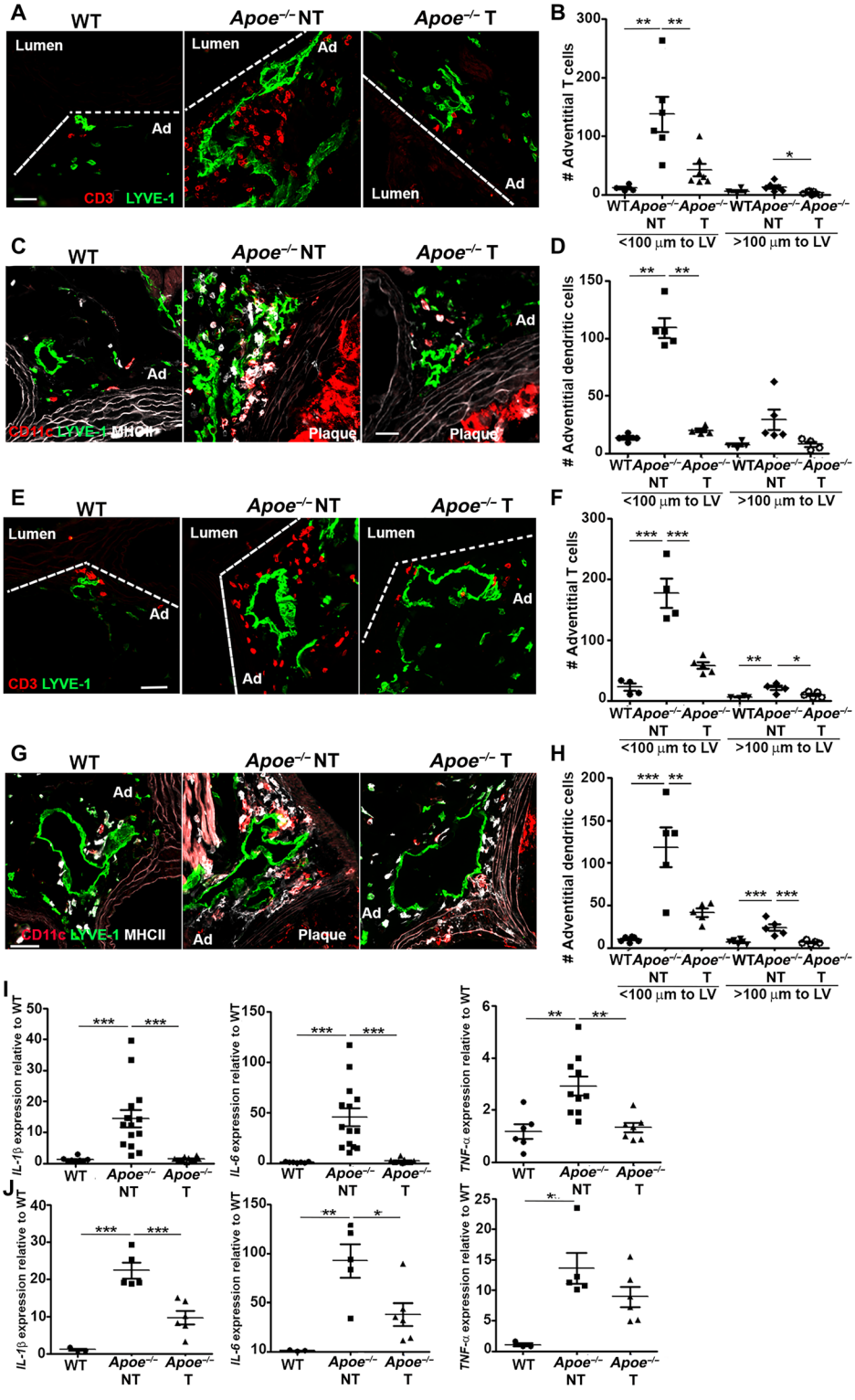

Fig. 3. Association of aortic lymphangiogenesis with immune cell accumulation and inflammation. Immunoreactivity for $CD3^+$ adventitial T cells was examined in aortic sinus from WT and *Apoe*$^{-/-}$ mice treated with ezetimibe [treated (T)] for (**A**) 12 weeks and (**E**) 16 weeks. Scale bar, 50 μm. The number of adventitial T cells within or outside a distance of 100 μm from the LVs was quantified in (**B**) 24-week-old and (**F**) 32-week-old NT WT, NT *Apoe*$^{-/-}$, and T *Apoe*$^{-/-}$ mice. Immunoreactivity for $CD11c^+MHCII^+$ adventitial DCs was examined in aortic sinus from (**C**) 24-week-old and (**G**) 32-week-old NT WT, NT *Apoe*$^{-/-}$, and T *Apoe*$^{-/-}$ mice. Scale bar, 50 μm. The number of adventitial DCs within or outside a distance of 100 μm from the LVs was quantified in (**D**) 24-week-old and (**H**) 32-week-old NT WT, NT *Apoe*$^{-/-}$, and T *Apoe*$^{-/-}$ mice. qPCR analysis of *IL-1*β, *IL-6*, and *TNF*-α was determined in aorta from NT WT, NT *Apoe*$^{-/-}$, and T *Apoe*$^{-/-}$ mice after (**I**) 12 weeks and (**J**) 16 weeks of treatment. $n = 4$ to 14 mice. One-way ANOVA was used for multiple group comparisons.

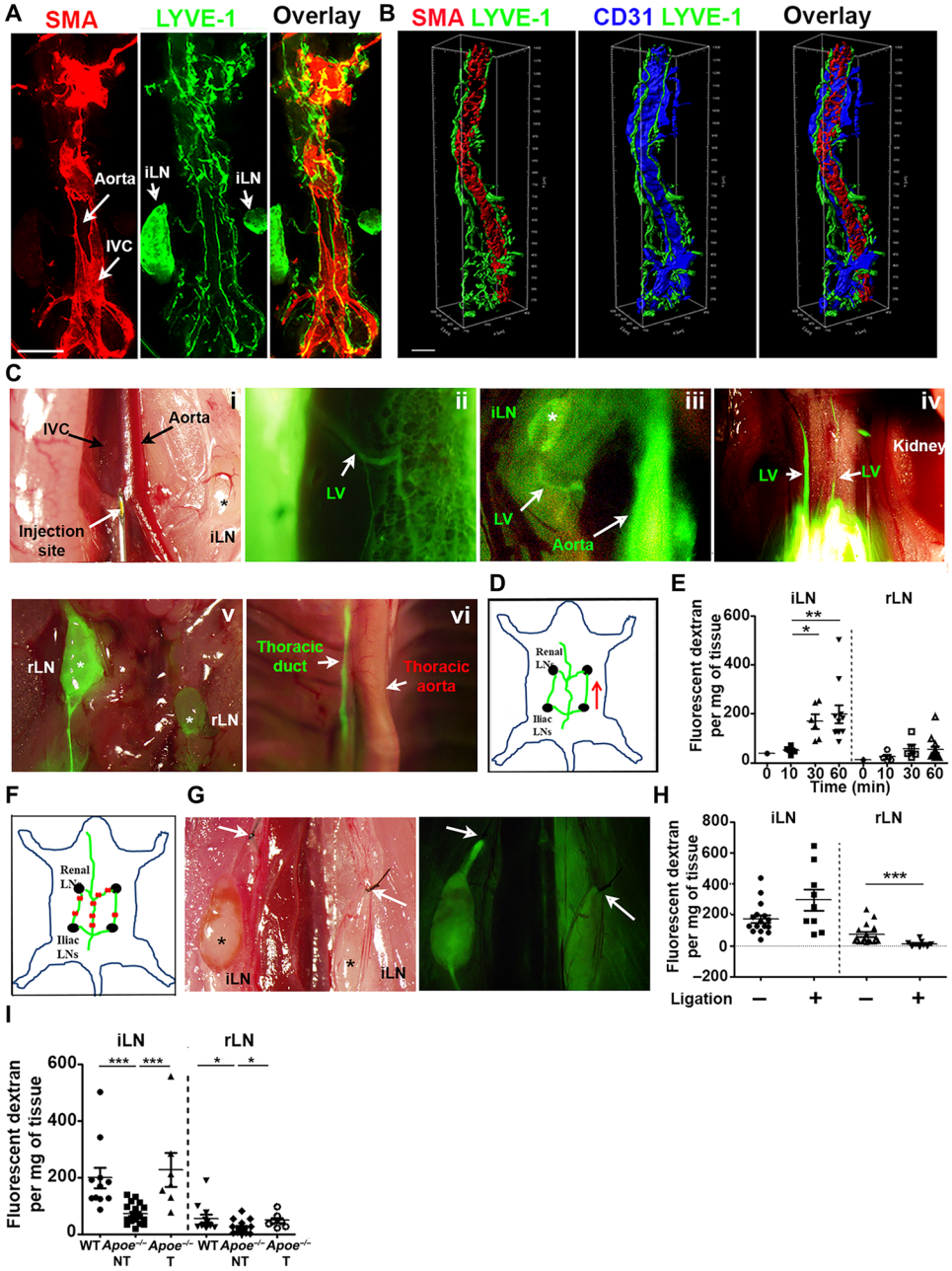

Fig. 4. Impaired lymphatic drainage during atherosclerosis. (**A**) Immunoreactivity for LYVE-1 and SMA was examined in whole-mount WT abdominal aorta (AA). LVs and iliac lymph nodes (iLNs) were positive for LYVE-1 expression. SMA fluorescence intensity in aorta was lower than in IVC and allowed differentiation between the aorta and the IVC. Scale bar, 500 μm. (**B**) 3D AA, IVC, and LVs from (A) were reconstructed using Imaris software. Scale bar, 100 μm. (**C**) Lymphatic transport of FITC-labeled dextran from aortic adventitia to thoracic duct was assessed. (i) FITC-labeled dextran injected from AA adventitia flowed through (ii) afferent lymphatic, (iii) iLNs, (iv) efferent lymphatic, (v) renal LNs (rLNs), and (vi) thoracic duct. Magnification: (i) ×0.7, (ii) ×5, (iii) ×0.7, (iv) ×2, (v) ×1.6, and (vi) ×1.25. (**D**) Schematic diagram depicts lymphatic transport of macromolecule (red arrow: flow direction). (**E**) FITC-labeled dextran transported to iLN and rLN in WT mice was quantified at 0, 10, 30, and 60 min after injection. (**F**) Schematic diagram and (**G**) images depict LV ligation in WT mice to disrupt LV flow. (**H**) FITC-labeled dextran transported to iLNs and rLNs in ligated and nonligated WT groups was quantified. (**I**) Quantification of FITC-labeled dextran transport to iLNs and rLNs was performed in WT, *Apoe*$^{-/-}$ mice treated with ezetimibe [treated (T)], or vehicle [nontreated (NT)]. $n = 1$ to 19 mice. One-way ANOVA was used for multiple group comparisons; otherwise, Mann-Whitney *U* test was used. Photo credit: Yeo Kim Pin, NUS.

lymphatic transport by measuring the fluorescence signal in iliac and renal LNs 10, 30, and 60 min following adventitial injection. Fluorescence intensity increased over time in both LNs, and the increase in iliac LNs became statistically significant 30 and 60 min after injection (Fig. 4E). We then selected the 60-min time point for subsequent assessment of lymphatic transport. We reasoned that if iliac and renal LNs are the draining LNs for abdominal aorta, the fluorescence tracer should increase in iliac LNs but decrease in renal LNs after injection when lymphatic drainage is interrupted between iliac and renal LNs. To test this hypothesis, we performed

aortic lymphatic ligation at multiple points including iliac efferent and renal afferent lymphatic vessels (Fig. 4F). Drainage of FITC-labeled dextran was blocked at the point of lymphatic ligation (Fig. 4G) and resulted in increased accumulation of fluorescent tracer in iliac LNs and in almost 90% reduction in renal LNs (Fig. 4H). Therefore, we concluded that iliac and renal LNs are the draining LNs of abdominal aorta. Having established a suitable quantitative approach to measure lymphatic drainage in aorta, we analyzed lymphatic transport in WT and *Apoe*$^{-/-}$ mice at ≥25 weeks old when lymphangiogenesis is evident and atherosclerosis is well advanced. We found that transport of FITC-labeled dextran from the abdominal aorta to the draining iliac and renal LNs was impeded by 64 and 56%, respectively, in *Apoe*$^{-/-}$ mice compared to WT mice (Fig. 4I). In contrast, ezetimibe-treated *Apoe*$^{-/-}$ mice exhibiting reduced atherosclerosis (fig. S4, B and C) and lymphangiogenesis (Fig. 2) showed a significant improvement in lymphatic drainage (Fig. 4I). Notably, treatment of *Apoe*$^{-/-}$ mice with VEGFC-156S enhanced lymphangiogenesis without affecting plasma cholesterol (fig. S5, C and D) but was not sufficient to restore lymphatic drainage because the accumulation of DC in adventitia was comparable to that in untreated *Apoe*$^{-/-}$ mice (fig. S5G). The size of atherosclerotic plaque was also unchanged in VEGFC-156S–treated *Apoe*$^{-/-}$ mice (fig. S5H). Together, these data demonstrate that despite the growth of lymphatic vessels in adventitia of atherosclerotic *Apoe*$^{-/-}$ mice, the lymphatic transport of macromolecule is sluggish during disease progression but is ameliorated during atherosclerosis regression. Thus, these provide evidence for lymph stasis in progressive atherosclerosis.

Aortic lymph stasis that resulted from lymphatic ligation promotes the development of atherosclerotic lesion

To functionally address the impact of impaired lymphatic drainage on atherosclerosis progression, we investigated the effect of ligating lymphatic vessels draining the abdominal aorta on plaque formation. Lymphatic ligation was performed on 12-week-old animals because at this age atherosclerotic lesions in abdominal aorta of *Apoe*$^{-/-}$ mice are negligible. A similar approach in *Apoe*$^{-/-}$ mice has been recently used by Rademakers *et al.* (*4*) to evaluate the role of adventitial lymphatic vessels in T cell accumulation. However, in their study, the authors analyzed the carotid artery of *Apoe*$^{-/-}$ mice where they placed a semiconstrictive collars to induce atherosclerosis after LN and lymphatic dissection. Here, we only ligated the aortic lymphatic vessels as described in Fig. 4F and allowed atherosclerosis to progress spontaneously for 4 weeks. At 4 weeks after ligation, lymph stasis significantly elevated the amount of total cholesterol in abdominal aorta without affecting total plasma cholesterol (Fig. 5A) and induced the intimal accumulation of CD68$^+$ macrophages and collagen and the loss of SMA in the media juxtaposed to the lesion (Fig. 5B). Atherosclerotic lesion size increased by 78% in ligated *Apoe*$^{-/-}$ mice compared to nonligated control animals (Fig. 5, C and D). In addition, CD3$^+$ T cell and CD11c$^+$MHCII$^+$ DC numbers were elevated in the intima and adventitia after lymphatic vessel ligation and correlated with plaque area (Fig. 5, E to H). We further examined whether abdominal aortic lymphatic ligation may affect adventitial inflammation. Assessment of inflammatory genes in adventitia from abdominal aorta after ligation showed significant increase in *IL-6* and *IL-1*β mRNA expression (Fig. 5I). Although lymphatic ligation did not promote the formation of atherosclerotic lesions in normocholesterolemic WT mice, it was sufficient to induce significant changes in the arterial wall. Four weeks after ligation, total plasma cholesterol levels remained unchanged, whereas aortic cholesterol levels were higher than sham control group (fig. S6A). Lymphatic ligation in WT mice also led to the adventitial accumulation of CD68$^+$ macrophages (fig. S6, B and C), CD3$^+$ T cells (fig. S6, D and E), and CD11c$^+$MHCII$^+$ DCs (fig. S6, F and G). Collectively, these interventional studies in *Apoe*$^{-/-}$ and WT mice indicate that functional lymphatic vessels are required for preventing adventitial inflammation and atherosclerosis progression by promoting the clearance of immune cells and cholesterol from the aortic wall.

Efficient lymphatic drainage is required for the regression of atherosclerosis mediated by ezetimibe

To further evaluate the implication of lymphatic drainage contribution to atherosclerosis, we investigated whether adequate lymphatic drainage is necessary to mediate regression of atherosclerosis by assessing the impact of aortic lymphatic ligation on the efficiency of ezetimibe treatment to reduce atherosclerosis. *Apoe*$^{-/-}$ mice were either treated with vehicle or ezetimibe from 32 weeks of age. One group of ezetimibe-treated animals was sham-operated, whereas the other group had its abdominal lymphatic vessels ligated. Atherosclerosis was analyzed 8 weeks after ligation and ezetimibe treatment in abdominal aorta and in innominate artery whose lymphatic vessels were not surgically ligated. Ligation of abdominal aortic lymphatic vessels in *Apoe*$^{-/-}$ mice altered neither the reduction of total plasma cholesterol levels induced by ezetimibe (Fig. 6A) nor atherosclerotic plaque cells, collagen content, and size in the innominate artery (fig. S7, A and B). In contrast, the ligation of abdominal lymphatic vessels significantly diminished the beneficial effects of ezetimibe treatment on atherosclerotic plaques developed in the abdominal aorta. Neutral lipids stained by oil red O, CD68$^+$ macrophages, SMA, and collagen content were increased in abdominal aortic lesions in ezetimibe-treated *Apoe*$^{-/-}$ mice with ligated lymphatic vessels compared to nonligated ezetimibe-treated mice (Fig. 6, B and C). Furthermore, the plaque area was significantly larger in ezetimibe-treated mice after lymphatic vessel ligation compared to nonligated ezetimibe-treated animals (Fig. 6D). These findings showed that the efficiency of the regression of atherosclerosis induced by ezetimibe treatment relies on a functional aortic lymphatic drainage.

DISCUSSION

Despite initial studies reporting an association between lymphangiogenesis and atherosclerosis, our study reveals that aortic lymphatic transport is impaired during atherosclerosis, and this sluggish lymphatic drainage contributes to atherosclerosis progression and adventitial inflammation. We showed in two atherosclerotic animal models that adventitial lymphangiogenesis occurs at later stages of plaque development. Reduction of hypercholesterolemia induced by ezetimibe reverses lymphangiogenesis and lymphatic morphological changes in *Apoe*$^{-/-}$ mice. Ezetimibe also diminished aortic *Vegf-c* mRNA expression in *Apoe*$^{-/-}$ mice. Furthermore, we found that increasing VEGF-C activity through VEGFC-156S treatment enhanced adventitial lymphangiogenesis in *Apoe*$^{-/-}$, whereas inhibiting it through VEGFR-3 blockade reduced lymphangiogenesis. Together, these findings suggest that hypercholesterolemia may trigger the lymphangiogenic response in *Apoe*$^{-/-}$ mice through a mechanism dependent, in part, on VEGF-C. However, we cannot exclude the involvement of other lymphangiogenic factors, immune cells, and inflammation. Mapping of the aortic lymphatic vessel network in

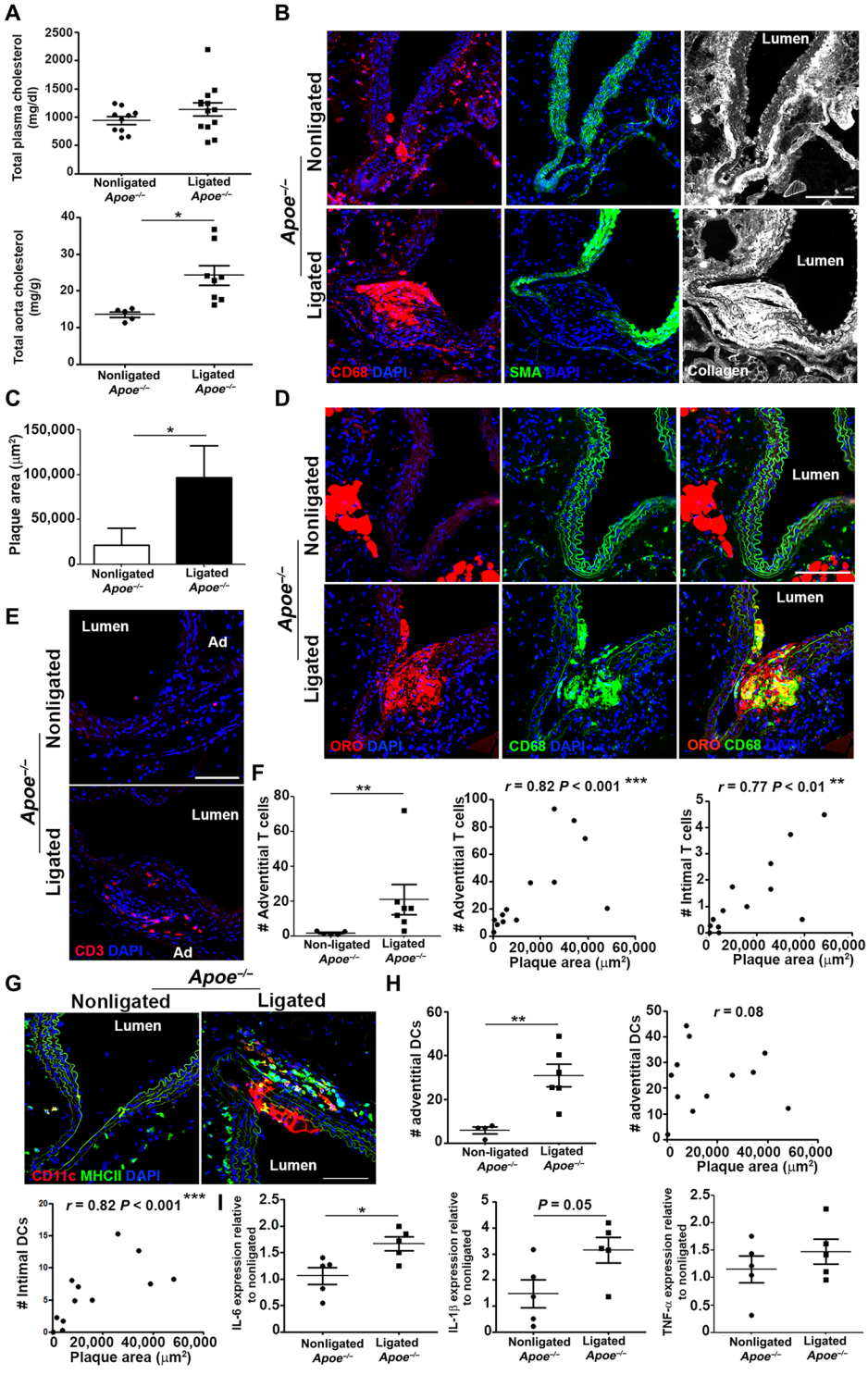

Fig. 5. Consequence of aortic lymphatic ligation on atherosclerosis development. (**A**) Total cholesterol levels were measured in plasma and abdominal aortae from nonligated and ligated *Apoe*$^{-/-}$ mice. (**B**) Immunoreactivity for CD68, SMA, and COLI was examined in abdominal aorta cross sections from nonligated and ligated *Apoe*$^{-/-}$ mice. DAPI, 4′,6-diamidino-2-phenylindole. (**C**) Total abdominal aorta atherosclerotic plaque area was quantified. (**D**) Abdominal aorta cross sections from nonligated and ligated *Apoe*$^{-/-}$ mice were costained with CD68 and oil red O. (**E**) Immunoreactivity for CD3^{+} T cells was examined in aorta cross sections from nonligated and ligated *Apoe*$^{-/-}$ mice. (**F**) The number of adventitial T cells and correlation of plaque area with adventitial and intimal T cell number from nonligated and ligated *Apoe*$^{-/-}$ mice were quantified. (**G**) Immunoreactivity for CD11c^{+}MHCII^{+} DCs was examined in aorta cross sections from nonligated and ligated *Apoe*$^{-/-}$ mice. (**H**) The number of adventitial DCs and correlation of plaque area with adventitial and intimal DC numbers were determined from nonligated and ligated *Apoe*$^{-/-}$ mice. Scale bar, 200 μm. (**I**) qPCR analysis of *IL-6*, *IL-1*β, and *TNF-*α was assessed in the aortic adventitia of nonligated and ligated *Apoe*$^{-/-}$ mice. $n = 4$ to 13 mice. Mann-Whitney *U* test and Student's *t* test were both used.

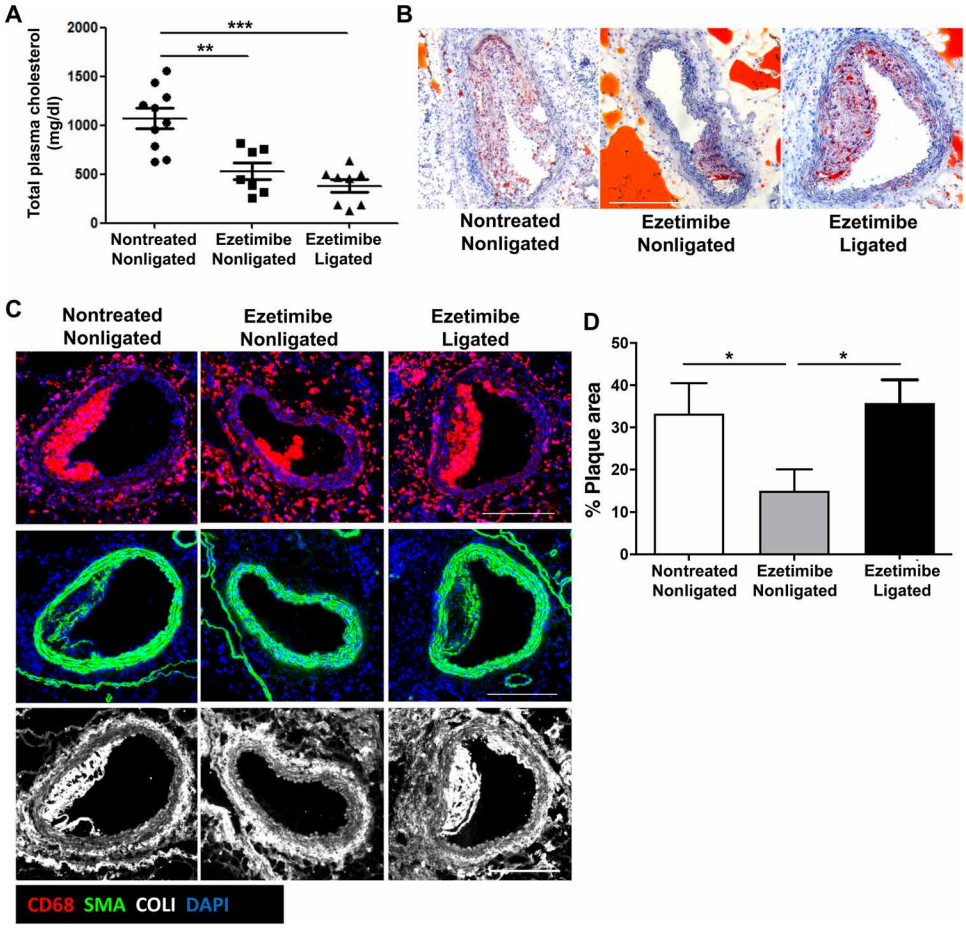

Fig. 6. Requirement of a functional lymphatic drainage for ezetimibe-induced atherosclerosis regression. (**A**) Total plasma cholesterol of vehicle-treated [nontreated (NT)] *Apoe*$^{-/-}$ and ezetimibe-treated (T) *Apoe*$^{-/-}$ mice that had undergone sham-operated (nonligated) or aortic lymphatic ligation (ligated) was measured. (**B**) Oil red O staining of abdominal aorta demonstrated larger plaque in ligated T *Apoe*$^{-/-}$ mice with increased lipid accumulation. Scale bar, 100 μm. (**C**) Immunoreactivity for CD68 (red), SMA (green), and COLI (white) was examined in abdominal aorta cross sections from nonligated NT *Apoe*$^{-/-}$, nonligated T *Apoe*$^{-/-}$, and ligated T *Apoe*$^{-/-}$ mice. Scale bar, 100 μm. (**D**) The total plaque area of abdominal aorta from nonligated NT *Apoe*$^{-/-}$, nonligated T *Apoe*$^{-/-}$, and ligated T *Apoe*$^{-/-}$ was quantified. $n = 4$ to 6 mice. Each point represents one mouse. Mann-Whitney *U* test was used.

WT and atherosclerotic mice using whole-mount staining and advanced clearing method also revealed that lymphatic vessels are not evenly distributed along the mouse aorta as shown by the paucity of adventitial lymphatic vessels in the aortic arch compared to aortic sinus and abdominal aorta. This spatial difference may explain the regression of adventitial lymphatic vessels observed in aortic arch of 32-week-old *Apoe*$^{-/-}$ mice fed an HFD reported by Taher *et al.* (*14*).

Although it is well documented that lymphangiogenesis occurs during chronic and acute inflammation (*24*), the biological role of lymphangiogenesis in inflammation remains poorly understood. Given the function of lymphatic vessels in cell trafficking and clearance of macromolecule, pathogen, and lipid, one would expect that lymphangiogenesis may constitute a positive response to inflammation by increasing lymph efflux and hence drainage of fluid, inflammatory mediators, and immune cells from the tissues into the draining LNs. However, few studies reported that inflammation-associated lymphangiogenesis is not always beneficial because the lymphatic vessels are not functional (*25*, *26*). For this reason, we thought that it was important to assess the functionality of lymphatic vessels draining the aorta during atherosclerosis. This had been believed to be technically impossible in mouse partly due to the small size of aorta diameter, poor knowledge of aortic lymphatic vessel anatomy, and absence of tools to directly inject molecular tracer in mouse aorta. As a consequence, most previous studies linking lymphatic function to atherosclerotic plaque formation investigated lymphatic transport in dermal tissue or peritoneal cavity and correlated it with atherosclerosis development. For instance, compromised transport of macromolecules by dermal lymphatic vessels, which can be improved by VEGF-C treatment, has been reported in *Apoe*$^{-/-}$ and *Ldlr*$^{-/-}$ mice (*19*, *27*). However, the response of lymphatic vessels to inflammation and atherogenic factors may vary depending on the organs or tissues. In line with this idea, the lymphatic dysfunction that we reported in skin of *Apoe*$^{-/-}$ and *Ldlr*$^{-/-}$ mice (*28*) was never associated with lymphangiogenesis. Similarly, VEGF-C expression is decreased in skin of *Apoe*$^{-/-}$ mice (*19*), whereas it is abundant in the aorta of these animals, as reported in this study and consistent with human coronary arteries (*10*, *11*). In this study, the three-dimensional (3D) visualization of lymphatic vessels in abdominal aorta allowed us to develop a method to quantitatively measure aortic lymphatic transport in mouse. Assessment

of transport of macromolecules by aortic lymphatics into the iliac and renal draining LNs provide direct evidence for lymph stasis in abdominal aorta of *Apoe*$^{-/-}$ mice compared to WT mice despite the expansion of lymphatic vessels. Aortic lymphatic drainage is ameliorated when atherosclerotic plaques and inflammation regress in response to ezetimibe, suggesting that hypercholesterolemia accounts, in part, for the lymphatic dysfunction, although the exact mechanism remains to be elucidated. The recent evidence that lymphatic endothelial cells express scavenger receptors for modified low-density lipoprotein including MSR-1 (SR-A1), MARCO (SR-A6), and CD36 suggest the possible direct effect of hypercholesterolemia on lymphatic function (*29*, *30*). However, hypercholesterolemia may also affect lymphatic vessel indirectly via, for example, the modulation of nitric oxide, which regulates lymphatic permeability (*31*). Although treatment with VEGFC-156S alone was able to enhance lymphangiogenesis without affecting hypercholesterolemia, it did not seem to be sufficient to improve lymphatic drainage and reduce atherosclerotic plaque size, further supporting the contribution of hypercholesterolemia in lymphatic dysfunction. It would be interesting to test whether targeting inflammation alone without affecting plasma cholesterol levels would be able to improve aortic lymphatic drainage. Our results further illustrate that the expansion of lymphatic vessels associated with inflammation may not always translate into the increase in lymphatic drainage, hence highlighting the importance of measuring lymphatic functionality to determine the biological significance of lymphangiogenesis in inflammatory diseases.

The clinical and experimental observations of high incidence of coronary artery diseases after mediastinal irradiation and enhanced atherosclerosis in pigs by mediastinal irradiation and high cholesterol diet led Lemole (*32*) to postulate in 1981 that lymph stasis could contribute to the development of coronary atherosclerosis. Recent studies in mouse hint toward this possible association between lymphatic transport and atherosclerosis. For instance, transgenic mouse models of lymphatic insufficiency (sVEGFR-3 and Chy mice) crossed with atherogenic mice (*Ldlr*$^{-/-}$ hApoB$^{100/100}$) display enhanced atherogenesis (*33*). Improving dermal lymphatic vessels by systemic administration of VEGF-C before the onset of atherosclerosis in *Ldlr*$^{-/-}$ mice attenuates the development of atherosclerosis (*27*). However, these studies did not investigate the function of aortic but peritoneal and/or dermal lymphatics. Here, we provide evidence for Lemole's hypothesis by demonstrating that lymphatic transport from the adventitia of the abdominal aorta to the draining LN is compromised in *Apoe*$^{-/-}$ mice and that ligation of adventitial lymphatic vessels before the onset of atherosclerosis promotes atherosclerotic plaque formation in this mouse model. Consistent with the latter finding, intimal thickening was observed after lymphatic ligation at the level of renal arteries in mongrel dogs (*34*). In lymphedema, lymph reflux and compromised forward lymph propulsion lead to fluid accumulation in the interstitium that further aggravates tissue inflammation. Notably, lymph stagnation in rat femoral vein induced by ligation of draining lymphatic collectors causes lipid retention, increased venous wall thickness, and TNF-α expression at the perivascular tissue (*35*). By analogy, lymph stasis in aorta may support inflammation in the arterial wall because ligation of adventitial lymphatic vessels in *Apoe*$^{-/-}$ mice induces intimal growth, adventitial inflammation, and accumulation of immune cells including DCs and T cells. Rademakers *et al.* (*4*) also showed that accumulation of T cells in atherosclerotic plaques induced by placing semiconstrictive collars in carotid arteries is aggravated after draining LN and lymphatic vessel dissection in *Apoe*$^{-/-}$ mice. These findings underscore the importance of adventitial lymphatic vessels in mediating the communication between intima and adventitia. While vascular inflammation in intima may affect the changes in adventitial environment ("inside-out" hypothesis), the view of "outside in," where failure in resolving adventitial inflammation contributes to advancing intimal atherosclerosis, should be considered (*2*). That the ligation of aortic lymphatic vessels in normocholesterolemic WT mice is sufficient to induce adventitia inflammation supports this idea. Aortic lymph stasis observed in *Apoe*$^{-/-}$ mice may also lead to atherosclerosis progression by interfering with the efficiency of reverse cholesterol transport, an atheroprotective mechanism dependent on lymphatic transport (*13*, *19*), as we observed accumulation of cholesterol in the arterial wall after lymphatic ligation. However, the contribution of aortic lymphatic vessel in reverse cholesterol transport has yet to be determined using a non-aorta transplantation model (*13*). Clearance of intimal lipoproteins and inflammatory cytokines through adventitial lymphatic vessels is likely plausible (*36*), but whether this may also apply to immune cells remains an open question in atherosclerosis field. It is not clear whether immune cells that are large in size can cross the media to reach adventitial lymphatic vessels.

Last, we demonstrated that efficient lymphatic drainage of the aorta is required for the therapeutic effect of ezetimibe on atherosclerotic plaque in mouse because ligation of adventitial lymphatic vessels significantly reduced the regression of atherosclerotic plaque induced by ezetimibe treatment in *Apoe*$^{-/-}$ mice. Because the ligation of adventitial lymphatic vessels did not compromise the lowering effect of ezetimibe on total plasma cholesterol but was still able to affect the regression of atherosclerotic plaque induced by ezetimibe, our data suggest that lymphatic drainage is an important determinant of plaque regression. Therefore, regression of the plaques might be maximal when circulating atherogenic factors such as cholesterol and inflammatory mediators are reduced and efficient aortic lymphatic drainage is promoted.

In summary, our work addresses previously unanswered question regarding the functionality of lymphatic vessels draining the aorta during atherosclerosis and its implication in disease progression. Because lymphatic drainage is compromised in atherosclerosis despite adventitial lymphangiogenesis, strategies improving lymphatic transport by, for example, targeting lymphatic collector function should be considered in conjunction with existing drugs as a treatment option for atherosclerosis.

MATERIALS AND METHODS

Mice and treatment

Apoe$^{-/-}$ and *Ldlr*$^{-/-}$ mice on a C57BL/6 background were obtained from The Jackson Laboratory (Bar Harbor, ME). WT and *Ldlr*$^{-/-}$ mice were maintained on an HFD (21% fat and 0.15% cholesterol) from 6 weeks of age. Twelve-week-old *Apoe*$^{-/-}$ mice received daily oral administration of ezetimibe (5 mg/kg per day) or vehicle (corn oil) for 12 or 16 weeks (*16*). In some experiments, 10-week-old *Apoe*$^{-/-}$ mice received 400 ng of VEGF-C and VEGFC-156S by intraperitoneal injection once every 3 days for 7 weeks (*19*). Signaling by VEGFR-3 was inhibited using selective blocking rat immunoglobulin G (IgG) from clone mF4-31C1 by intraperitoneal injection at a dose of 0.8 mg per mouse every alternate day for 12 weeks (*37*). Mice were housed within Satellite Animal Housing Unit of the

National University of Singapore. All experimental procedures performed were approved by the institutional animal care and use committees of the National University of Singapore.

Immunohistochemistry

Aortic sinus, innominate artery, and abdominal aorta were either freshly embedded in tissue-freezing medium or fixed in 2% paraformaldehyde/30% sucrose solution at 4°C and embedded in tissue-freezing medium. Seven-micrometer-thick cryostat sections were cut for imaging by fluorescence microscopy. Primary antibodies used included rabbit anti-mouse LYVE-1 (Abcam), Armenian hamster anti-mouse CD31 (Millipore), rabbit anti-mouse type I collagen (Millipore), rat anti-mouse CD31 (BD Pharmingen), rat anti-mouse CD68 (Serotec), FITC-conjugated monoclonal α-SMA (Sigma-Aldrich), Cy3-conjugated monoclonal α-SMA (Sigma-Aldrich), goat anti-mouse VEGFR-3 (R&D Systems), rat anti-mouse Ki67 (Dako), rabbit anti-mouse prox-1 (AngioBio), hamster anti-mouse podoplanin (clone 8.1.1, Developmental Studies Hybridoma Bank, University of Iowa, Iowa City, IA), rat anti-mouse MHCII (eBioscience), Armenian hamster anti-mouse CD11c (eBioscience), Armenian hamster anti-mouse CD3e (eBioscience), rat anti-mouse IgG2a (eBioscience), rabbit anti-mouse IgG (Jackson ImmunoResearch Laboratories), and goat anti-mouse IgG (Jackson ImmunoResearch Laboratories). Secondary antibodies conjugated with DyLight 549, DyLight 647, Alexa Fluor 488, Cy2, and Cy3 (Jackson ImmunoResearch Laboratories) were used for detection. Sections were counterstained with 4,6-diamidino-2-phenylindole for cell nuclei visualization and mounted for analysis. For histological analysis of lipid, sections were stained with oil red O. For identification of lipid-laded macrophages, sections were stained with macrophage marker rat anti-mouse CD68 (Serotec), followed by oil red O staining, which was visualized as pseudo-colored red under the Texas Red filter.

For whole-mount staining, aortae dissected from WT, *Apoe*$^{-/-}$, and *Ldlr*$^{-/-}$ mice were fixed with 2% paraformaldehyde and blocked with phosphate-buffered saline (PBS) containing 0.3% Triton X-100 and 0.5% bovine serum albumin. For immunofluorescent whole-mount staining, samples were incubated with primary antibodies, followed by incubating with secondary antibodies. Some samples were further cleared with RapiClear 1.52 (Sun Jin Lab) for 30 min or until samples were transparent. For colorimetric detection, aortic sinuses were first incubated with 3% (v/v) hydrogen peroxide for 1 hour before blocking and primary antibody staining. Aortic sinuses were then stained with horseradish peroxidase–conjugated secondary antibody, and whole-mount tissue was then developed and revealed using an ImmPACT DAB peroxidase substrate (Vector Laboratories). Images were captured with a fluorescence dissecting microscope (Olympus, SZX16). For some aortic sinus whole mount, samples were mounted on a slide with Dako fluorescent mounting medium and coverslip and then viewed with a confocal microscope (Leica TCS SP5, Leica Microsystems Inc., Deerfield, IL) with LAS AF confocal software (version 1.8.2, Leica Microsystems Inc.) or fluorescence dissecting microscope (Olympus, SZX16).

For ultramicroscopy, aortae were embedded in 1% low-melting temperature agarose gel and cleared using the benzyl alcohol, benzyl benzoate (BABB) protocol. Samples were serially dehydrated in methanol with grades of 50, 70, 95, and 100% (2 hours for each methanol grade). Dehydrated aortae were equilibrated in BABB:methanol in a 1:1 ratio and refractive index–matched with BABB (1:2) for 2 hours until clear. Cleared aortae were imaged using light sheet UltraMicroscope I (LaVision BioTec GmbH, Bielefeld, Germany) using a supercontinuum white light laser for excitation. Alexa Fluor 488 was imaged using 470/40 excitation and 525/50 emission bandpass filters (Semrock), and Cy3 was imaged using 560/30 excitation and 620/60 emission bandpass filters (Semrock). Imaging was performed at ×2 magnification.

Image analysis

The entire aortic sinus, innominate artery, and abdominal aorta were sectioned through in sequence, and immunofluorescence analysis was performed and quantified on every alternate slide in sequence. Adventitial CD31^{+}LYVE-1^{+}CD68^{-} lymphatic vessels, CD31^{+}LYVE-1^{-}CD68^{-} blood vessel number, CD11c^{+}MHCII^{+} DCs, and CD3^{+} T cells were counted per aortic sinus cross section. Three to 10 sections per aortic sinus were quantified, and each section was 45 μm apart. For atherosclerotic lesion analysis, total intimal lesion area identified by CD68, SMA, and collagen I in each cross section was quantified by taking the average of at least six sections spaced 45 μm apart. The total DC area was quantified using ImageJ software, as the total amount of CD11c^{+} DCs was found in the entire LN. For whole-mount samples, images were analyzed using ImageJ software. A 3D image analysis and volume rendering of confocal z-stacks images were processed using Imaris software (version 9.0.2, Bitplane).

Quantitative real-time PCR

Whole aorta and adventitia of aortic sinus were collected in RNAlater (Qiagen). The total RNA from tissues was homogenized and extracted using TRIzol reagent (Qiagen) and a NucleoSpin RNA II kit (Macherey-Nagel) or a Qiagen RNeasy Micro kit according to the manufacturer's instructions. For aortic adventitia, it was kept in lysis binding buffer and the total mRNA was isolated from cells using a mirVana miRNA isolation kit (Life Technologies) according to the manufacturer's instructions. Complementary DNA (cDNA) was amplified and synthesized using Ovation PicoSL WTA System V2 (NuGEN) according to the manufacturer's instructions. cDNA concentrations and purity were measured using the NanoDrop 1000 Spectrophotometer (Thermo Fisher Scientific). Real-time quantitative polymerase chain reaction (qPCR) was performed using SYBR

Table 1. List of primers used for quantitative real-time PCR.

Target genes	Primer sequence
Prox-1	Forward: 5′-CTCTCCATCACCAGGGATTG-3′
	Reverse: 5′-CCTTGTAAATGGCCTTCTTCC-3′
IL-1β	Forward: 5′-CTTCAAATCTCGCAGCAGCACATC-3′
	Reverse: 5′-CCAGCAGGTTATCATCATCATCC-3′
IL-6	Forward: 5′-GTTGCCTTCTTGGGACTGAT-3′
	Reverse: 5′-GCCATTGCACAACTCTTTTCT-3′
TNF-α	Forward: 5′-CTGTAGCCCACGTCGTAGCAAACC-3′
	Reverse: 5′-CGGCTGACGGTGTGGGTGAG-3′
GAPDH	Forward: 5′-TGCGACTTCAACAGCAACTC-3′
	Reverse: 5′-ATGTAGGCCATGAGGTCCAC-3′
R12s	Forward: 5′-GGAAGGCATAGTGCTGGAGGT-3′
	Reverse: 5′-CGATGACATCCTTGGCCTGA-3′

Green PCR Master Mix (Applied Biosystems) and analyzed on the ABI Prism 7500 Detection System (Applied Biosystems, Warrington, UK). Gene expression was normalized to glyceraldehyde-3-phosphate dehydrogenase (GAPDH) or r12S expression. qPCR analysis of *Prox-1* gene was performed in one pool of adventitia from four WT aortic sinuses ($n = 1$) and three pools of adventitia from four $Apoe^{-/-}$ aortic sinuses ($n = 3$). The primer sequences are listed in Table 1.

Microlymphangiography of aortic lymphatic vessel

To analyze the ability of lymphatics to transport macromolecule, fluorescent tracer was injected at the adventitia of abdominal aorta, specifically at the region between the aorta and IVC and before aortic bifurcation. Mice were sedated with intraperitoneal injection of ketamine (100 mg/kg) and xylazine (10 mg/kg) for the duration of the microlymphangiography. Four microliters of 70-kDa FITC-labeled dextran (Molecular Probes) was injected and visualized under a fluorescence dissecting microscope. To quantify the lymphatic transport of FITC-labeled dextran, iliac and renal LNs were isolated 10, 30, and 60 min after injection. LNs were homogenized with 120 µl of PBS and quantified at an excitation of 490 nm and emission of 520 nm. Data were expressed as fluorescence intensity per microgram of tissue weight. Samples from mice injected with 4 µl of PBS and processed as above were used as blanks.

Aortic vessel ligation

To evaluate the effect of lymphatic ligation on aorta and atherosclerosis, sham-operated and aortic lymphatic ligation were performed on HFD-fed WT and $Apoe^{-/-}$ mice aged 12 weeks old. All mice were fed on an HFD until analysis 4 weeks after ligation. For ezetimibe-treated $Apoe^{-/-}$ mice, ligation was performed at 32 weeks old, followed by 8 weeks of ezetimibe treatment before harvest. Briefly, mice were injected subcutaneously with buprenorphine (0.2 to 1 mg/kg) and enrofloxacin (20 mg/kg) before surgery. Mice were anesthetized with 3 to 5% isoflurane and maintained with 1.5% isoflurane during the removal of abdominal hair and during the entire ligation procedure. After disinfecting the abdominal skin with povidone-iodine, a middle abdominal incision was made and the abdominal organs were retracted outside of the abdomen with sterile gauze to expose the abdominal aorta. Lymphatic vessels draining the aorta were identified on the basis of their translucent appearance, and multiple ligation points were made using 11-0 suture. The abdominal incision was closed in two layers with 6-0 sutures, and mice were allowed to recover on a heating pad. All mice were monitored and administered subcutaneously with buprenorphine and enrofloxacin for 3 days.

Statistical analysis

Statistical analysis was performed with Prism 7 (GraphPad Software). The tests applied are indicated in the figure legends. Data are represented as mean ± SEM. Statistical significances were determined using the unpaired two-tailed *t* test and nonparametric Mann-Whitney *U* test. A one-way analysis of variance (ANOVA) was used to compare multiple groups with one experimental parameter. A *P* value of less than 0.05 was considered to be statistically significant. $^{*}P < 0.05$, $^{**}P < 0.01$, and $^{***}P < 0.0001$.

SUPPLEMENTARY MATERIALS

Supplementary material for this article is available at http://advances.sciencemag.org/cgi/content/full/6/50/eabc2697/DC1

View/request a protocol for this paper from *Bio-protocol*.

REFERENCES AND NOTES

1. C. K. Glass, J. L. Witztum, Atherosclerosis. The road ahead. *Cell* **104**, 503–516 (2001).
2. K. Maiellaro, W. R. Taylor, The role of the adventitia in vascular inflammation. *Cardiovasc. Res.* **75**, 640–648 (2007).
3. K. Vaahtomeri, S. Karaman, T. Mäkinen, K. Alitalo, Lymphangiogenesis guidance by paracrine and pericellular factors. *Genes Dev.* **31**, 1615–1634 (2017).
4. T. Rademakers, E. P. C. van der Vorst, I. T. M. N. Daissormont, J. J. T. Otten, K. Theodorou, T. L. Theelen, M. Gijbels, A. Anisimov, H. Nurmi, J. H. N. Lindeman, A. Schober, S. Heeneman, K. Alitalo, E. A. L. Biessen, Adventitial lymphatic capillary expansion impacts on plaque T cell accumulation in atherosclerosis. *Sci. Rep.* **7**, 45263 (2017).
5. K. Drozdz, D. Janczak, P. Dziegiel, M. Podhorska, D. Patrzałek, P. Ziółkowski, R. Andrzejak, A. Szuba, Adventitial lymphatics of internal carotid artery in healthy and atherosclerotic vessels. *Folia Histochem. Cytobiol.* **46**, 433–436 (2008).
6. K. Drozdz, D. Janczak, P. Dziegiel, M. Podhorska, A. Piotrowska, D. Patrzalek, R. Andrzejak, A. Szuba, Adventitial lymphatics and atherosclerosis. *Lymphology* **45**, 26–33 (2012).
7. I. Kutkut, M. J. Meens, T. A. McKee, M.-L. Bochaton-Piallat, B. R. Kwak, Lymphatic vessels: An emerging actor in atherosclerotic plaque development. *Eur. J. Clin. Invest.* **45**, 100–108 (2015).
8. G. Csányi, B. Singla, Arterial lymphatics in atherosclerosis: Old questions, new insights, and remaining challenges. *J. Clin. Med.* **8**, 495 (2019).
9. I. Kholová, G. Dragneva, P. Cermáková, S. Laidinen, N. Kaskenpää, T. Hazes, E. Cermáková, I. Steiner, S. Ylä-Herttuala, Lymphatic vasculature is increased in heart valves, ischaemic and inflamed hearts and in cholesterol-rich and calcified atherosclerotic lesions. *Eur. J. Clin. Invest.* **41**, 487–497 (2011).
10. O. Eliska, M. Eliskova, A. J. Miller, The absence of lymphatics in normal and atherosclerotic coronary arteries in man: A morphologic study. *Lymphology* **39**, 76–83 (2006).
11. T. Nakano, Y. Nakashima, Y. Yonemitsu, S. Sumiyoshi, Y.-X. Chen, Y. Akishima, T. Ishii, M. Iida, K. Sueishi, Angiogenesis and lymphangiogenesis and expression of lymphangiogenic factors in the atherosclerotic intima of human coronary arteries. *Hum. Pathol.* **36**, 330–340 (2005).
12. E. Brakenhielm, K. Alitalo, Cardiac lymphatics in health and disease. *Nat. Rev. Cardiol.* **16**, 56–68 (2019).
13. C. Martel, W. Li, B. Fulp, A. M. Platt, E. L. Gautier, M. Westerterp, R. Bittman, A. R. Tall, S.-H. Chen, M. J. Thomas, D. Kreisel, M. A. Swartz, M. G. Sorci-Thomas, G. J. Randolph, Lymphatic vasculature mediates macrophage reverse cholesterol transport in mice. *J. Clin. Invest.* **123**, 1571–1579 (2013).
14. M. Taher, S. Nakao, S. Zandi, M. I. Melhorn, K. C. Hayes, A. Hafezi-Moghadam, Phenotypic transformation of intimal and adventitial lymphatics in atherosclerosis: A regulatory role for soluble VEGF receptor 2. *FASEB J.* **30**, 2490–2499 (2016).
15. H. Y. Lim, S. Y. Lim, C. K. Tan, C. H. Thiam, C. C. Goh, D. Carbajo, S. H. S. Chew, P. See, S. Chakarov, X. N. Wang, L. H. Lim, L. A. Johnson, J. Lum, C. Y. Fong, A. Bongso, A. Biswas, C. Goh, M. Evrard, K. P. Yeo, R. Basu, J. K. Wang, Y. Tan, R. Jain, S. Tikoo, C. Choong, W. Weninger, M. Poidinger, R. E. Stanley, M. Collin, N. S. Tan, L. G. Ng, D. G. Jackson, F. Ginhoux, V. Angeli, Hyaluronan receptor LYVE-1-expressing macrophages maintain arterial tone through hyaluronan-mediated regulation of smooth muscle cell collagen. *Immunity* **49**, 326–341.e7 (2018).
16. H. R. Davis Jr., D. S. Compton, L. Hoos, G. Tetzloff, Ezetimibe, a potent cholesterol absorption inhibitor, inhibits the development of atherosclerosis in ApoE knockout mice. *Arterioscler. Thromb. Vasc. Biol.* **21**, 2032–2038 (2001).
17. P. J. Kuhlencordt, P. Padmapriya, S. Rützel, J. Schödel, K. Hu, A. Schäfer, P. L. Huang, G. Ertl, J. Bauersachs, Ezetimibe potently reduces vascular inflammation and arteriosclerosis in eNOS-deficient ApoE ko mice. *Atherosclerosis* **202**, 48–57 (2009).
18. M. H. Ahmed, C. D. Byrne, Potential therapeutic uses for ezetimibe beyond lowering LDL-c to decrease cardiovascular events. *Diabetes Obes. Metab.* **12**, 958–966 (2010).
19. H. Y. Lim, C. H. Thiam, K. P. Yeo, R. Bisoendial, C. S. Hii, K. C. Y. McGrath, K. W. Tan, A. Heather, J. S. J. Alexander, V. Angeli, Lymphatic vessels are essential for the removal of cholesterol from peripheral tissues by SR-BI-mediated transport of HDL. *Cell Metab.* **17**, 671–684 (2013).
20. M. H. D. Tay, S. Y. J. Lim, Y. F. I. Leong, C. H. Thiam, K. W. Tan, F. T. Torta, P. Narayanaswamy, M. Wenk, V. Angeli, Halted lymphocyte egress via efferent lymph contributes to lymph node hypertrophy during hypercholesterolemia. *Front. Immunol.* **10**, 575 (2019).
21. H. Wada, S. Ura, S. Kitaoka, N. Satoh-Asahara, T. Horie, K. Ono, T. Takaya, R. Takanabe-Mori, M. Akao, M. Abe, T. Morimoto, T. Murayama, M. Yokode, M. Fujita, A. Shimatsu, K. Hasegawa, Distinct characteristics of circulating vascular endothelial growth factor-A and C levels in human subjects. *PLOS ONE* **6**, e29351 (2011).
22. V. Joukov, V. Kumar, T. Sorsa, E. Arighi, H. Weich, O. Saksela, K. Alitalo, A recombinant mutant vascular endothelial growth factor-C that has lost vascular endothelial growth factor receptor-2 binding, activation, and vascular permeability activities. *J. Biol. Chem.* **273**, 6599–6602 (1998).

23. M. Weber, M. Sixt, Live cell imaging of chemotactic dendritic cell migration in explanted mouse ear preparations. *Methods Mol. Biol.* **1013**, 215–226 (2013).
24. H. Kim, R. P. Kataru, G. Y. Koh, Inflammation-associated lymphangiogenesis: A double-edged sword? *J. Clin. Invest.* **124**, 936–942 (2014).
25. B.-H. Jeon, C. Jang, J. Han, R. P. Kataru, L. Piao, K. Jung, H. J. Cha, R. A. Schwendener, K. Y. Jang, K.-S. Kim, K. Alitalo, G. Y. Koh, Profound but dysfunctional lymphangiogenesis via vascular endothelial growth factor ligands from CD11b+ macrophages in advanced ovarian cancer. *Cancer Res.* **68**, 1100–1109 (2008).
26. T. F. Wu, C. J. Carati, W. K. MacNaughton, P.-Y. von der Weid, Contractile activity of lymphatic vessels is altered in the TNBS model of guinea pig ileitis. *Am. J. Physiol. Gastrointest. Liver Physiol.* **291**, G566–G574 (2006).
27. A. Milasan, A. Smaani, C. Martel, Early rescue of lymphatic function limits atherosclerosis progression in *Ldlr*$^{-/-}$ mice. *Atherosclerosis* **283**, 106–119 (2019).
28. H. Y. Lim, J. M. Rutkowski, J. Helft, S. T. Reddy, M. A. Swartz, G. J. Randolph, V. Angeli, Hypercholesterolemic mice exhibit lymphatic vessel dysfunction and degeneration. *Am. J. Pathol.* **175**, 1328–1337 (2009).
29. N. Fujimoto, Y. He, M. D'Addio, C. Tacconi, M. Detmar, L. C. Dieterich, Single-cell mapping reveals new markers and functions of lymphatic endothelial cells in lymph nodes. *PLOS Biol.* **18**, e3000704 (2020).
30. S. J. Berendam, A. F. Koeppel, N. R. Godfrey, S. J. Rouhani, A. N. Woods, A. B. Rodriguez, J. D. Peske, K. L. Cummings, S. D. Turner, V. H. Engelhard, Comparative transcriptomic analysis identifies a range of immunologically related functional elaborations of lymph node associated lymphatic and blood endothelial cells. *Front. Immunol.* **10**, 816 (2019).
31. J. P. Scallan, M. A. Hill, M. J. Davis, Lymphatic vascular integrity is disrupted in type 2 diabetes due to impaired nitric oxide signalling. *Cardiovasc. Res.* **107**, 89–97 (2015).
32. G. M. Lemole, The role of lymphstasis in atherogenesis. *Ann. Thorac. Surg.* **31**, 290–293 (1981).
33. T. Vuorio, H. Nurmi, K. Moulton, J. Kurkipuro, M. R. Robciuc, M. Öhman, S. E. Heinonen, H. Samaranayake, T. Heikura, K. Alitalo, S. Ylä-Herttuala, Lymphatic vessel insufficiency in hypercholesterolemic mice alters lipoprotein levels and promotes atherogenesis. *Arterioscler. Thromb. Vasc. Biol.* **34**, 1162–1170 (2014).
34. Y. Nakata, S. Shionoya, Structure of lymphatics in the aorta and the periaortic tissues, and vascular lesions caused by disturbance of the lymphatics. *Lymphology* **12**, 18–19 (1979).
35. H. Tanaka, N. Zaima, T. Sasaki, N. Yamamoto, M. Sano, H. Konno, M. Setou, N. Unno, Loss of lymphatic vessels and regional lipid accumulation is associated with great saphenous vein incompetence. *J. Vasc. Surg.* **55**, 1440–1448 (2012).
36. B. G. Nordestgaard, E. Hjelms, S. Stender, K. Kjeldsen, Different efflux pathways for high and low density lipoproteins from porcine aortic intima. *Arteriosclerosis* **10**, 477–485 (1990).
37. K. W. Tan, K. P. Yeo, F. H. S. Wong, H. Y. Lim, K. L. Khoo, J.-P. Abastado, V. Angeli, Expansion of cortical and medullary sinuses restrains lymph node hypertrophy during prolonged inflammation. *J. Immunol.* **188**, 4065–4080 (2012).

Acknowledgments: We would like to thank the mouse core service group at Singapore Immunology Network and comparative medicine at the National University of Singapore for technical support. We thank E. C. Martinez for teaching us laparotomy procedure and H. C. Shii for contribution to this work. We are grateful to B. Pytowski (ImClone Systems) for the gift of anti–VEGFR-3 antibodies. **Funding:** This work was supported by NMRC (IRG10May071) and MOE (MOET15-T2-1-019) grants and the National Research Foundation, Prime Minister's Office, Singapore, under its Campus for Research Excellence and Technological Enterprise (CREATE) program to V.A. **Author contributions**: K.P.Y. conceived, designed, and performed the experiments; analyzed primary and aggregated data; and wrote the manuscript. A.B. and Y. Tang performed and analyzed light sheet ultramicroscopic imaging. C.H.T., W.Q.S., Y. Tan, X.H.K., H.S.C., and M.H.Z. performed and analyzed some experiments. M.L.P. commented on the aortic lymphatic function technique. H.Y.L., C.T., and S.H.A. performed sectioning and immunostaining. S.Y.L. performed animal postsurgical monitoring. L.G.N. provided reagents and commented on light sheet ultramicroscopy imaging results. H.Y.L. commented on the manuscript. V.A. conceived and supervised the project, designed experiments, analyzed aggregated data, and wrote and edited the manuscript. **Competing interests:** The authors declare that they have no competing interests. **Data and materials availability:** All data needed to evaluate the conclusions in the paper are present in the paper and/or the Supplementary Materials. Additional data related to this paper may be requested from the authors.

Submitted 15 April 2020
Accepted 22 October 2020
Published 11 December 2020
10.1126/sciadv.abc2697

Citation: K. P. Yeo, H. Y. Lim, C. H. Thiam, S. H. Azhar, C. Tan, Y. Tang, W. Q. See, X. H. Koh, M. H. Zhao, M. L. Phua, A. Balachander, Y. Tan, S. Y. Lim, H. S. Chew, L. G. Ng, V. Angeli, Efficient aortic lymphatic drainage is necessary for atherosclerosis regression induced by ezetimibe. *Sci. Adv.* **6**, eabc2697 (2020).